Cell

Reprogramming Adult Schwann Cells to Stem Cell-like Cells by Leprosy Bacilli Promotes Dissemination of Infection

Toshihiro Masaki,[1,2,4] Jinrong Qu,[4] Justyna Cholewa-Waclaw,[1,2] Karen Burr,[2] Ryan Raaum,[4] and Anura Rambukkana[1,2,3,4,*]
[1]MRC Center for Regenerative Medicine
[2]Center for Neuroregeneration
[3]Center for Infectious Diseases
University of Edinburgh, Little France Campus, Edinburgh, EH16 4UU Scotland, UK
[4]The Rockefeller University, York Avenue, New York, NY 10065, USA
*Correspondence: a.rambuka@ed.ac.uk
http://dx.doi.org/10.1016/j.cell.2012.12.014

SUMMARY

Differentiated cells possess a remarkable genomic plasticity that can be manipulated to reverse or change developmental commitments. Here, we show that the leprosy bacterium hijacks this property to reprogram adult Schwann cells, its preferred host niche, to a stage of progenitor/stem-like cells (pSLC) of mesenchymal trait by downregulating Schwann cell lineage/differentiation-associated genes and upregulating genes mostly of mesoderm development. Reprogramming accompanies epigenetic changes and renders infected cells highly plastic, migratory, and immunomodulatory. We provide evidence that acquisition of these properties by pSLC promotes bacterial spread by two distinct mechanisms: direct differentiation to mesenchymal tissues, including skeletal and smooth muscles, and formation of granuloma-like structures and subsequent release of bacteria-laden macrophages. These findings support a model of host cell reprogramming in which a bacterial pathogen uses the plasticity of its cellular niche for promoting dissemination of infection and provide an unexpected link between cellular reprogramming and host-pathogen interaction.

INTRODUCTION

Differentiated adult cells are natural targets for many intracellular bacterial pathogens. These pathogens often establish infection in their preferred niches by manipulating or subverting differentiated host cell functions (Falkow, 1991). Although it is now recognized that these cells posses unprecedented genomic plasticity and nuclear reprogramming potential (Wilmut et al., 1997; Gurdon, 1962; Gurdon and Melton, 2008; Theise and Wilmut, 2003; Takahashi and Yamanaka, 2006) it is not known whether bacterial pathogens have coevolved to leverage such host cell plasticity for their advantage. Among differentiated cells, Schwann cells, the glial cells of the adult peripheral nervous system (PNS) that are comprised of myelin-forming and non-myelin-forming phenotypes (Jessen and Mirsky, 2005), show remarkable plasticity and contribute to the regeneration capacity of the adult PNS even after severe injury (Fawcett and Keynes, 1990). *Mycobacterium leprae* (ML), which causes human leprosy, establishes infection in adult Schwann cells, a primary nonimmune target, and causes subsequent neurological injury, leading to sensorimotor loss (Job, 1989; Shetty et al., 1988; Stoner, 1979).

Although ML infection in humans initially presents with inflammation-mediated sensorimotor loss (Job, 1989; Miko et al., 1993; Scollard et al., 2006; Stoner, 1979), the early events of PNS infection in human are unknown. ML is a strictly obligate intracellular pathogen with a severely decayed bacterial genome and is totally dependent on host cell functions for survival (Cole et al., 2001). Recent studies have suggested that ML uses the regeneration properties of the PNS for expansion of the bacterial niche within Schwann cells (Rambukkana et al., 2002, 2010; Tapinos et al., 2006). In patients with advanced leprosy, regeneration of damaged peripheral nerves has been documented despite the bacterial presence (Miko et al., 1993). This may also reflect the bacterial efforts to secure and propagate the Schwann cell niche during human infection. Thus, once invaded, ML uses strategies that promote Schwann cell endurance or rejuvenation in order to maintain infected cells in active stage so that essential host factors critical for bacterial survival can be acquired. In addition, Schwann cells also serve as a safe haven for ML, as the PNS blood-nerve barrier protects ML from host immune assault (Job, 1989; Stoner, 1979). Such favorable conditions, which are assisted with the nontoxic, noncytopathic, non-apoptotic, and nontumorigenic nature of ML, permit bacterial residence within host cells for a long period (Lahiri et al., 2010; Tapinos and Rambukkana, 2005).

The bacillary load in Schwann cells is a critical determinant for the subsequent immunopathology that manifests in various tissues following ML dissemination (Miko et al., 1993). After Schwann cell colonization, leprosy bacilli need an exit route in

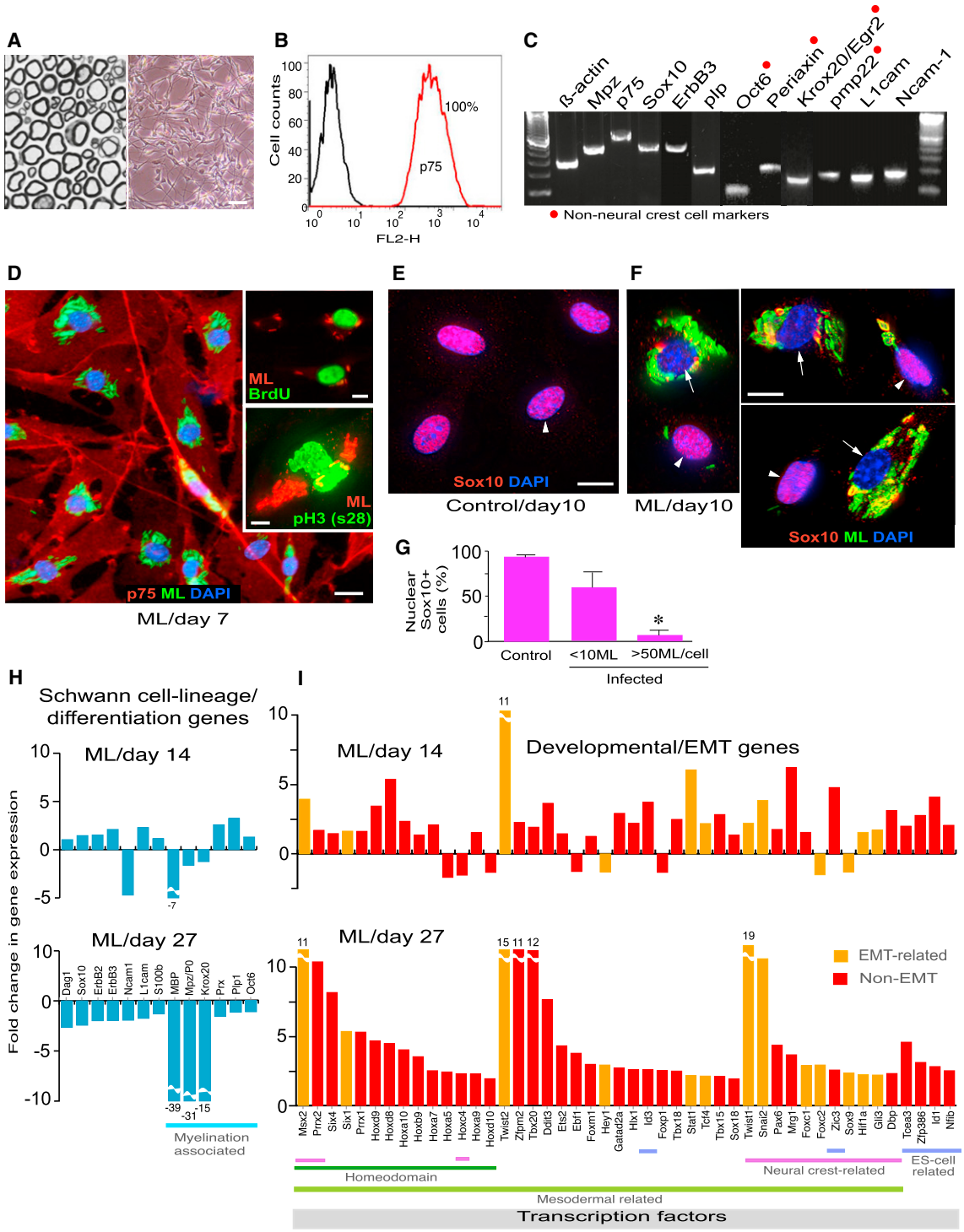

Figure 1. Adult Peripheral Nerve-Derived Schwann Cells Undergo Reprogramming Events in Response to Intracellular ML

(A and B) Methylin-blue-stained semithin section of adult nerves (A, left) from which Schwann cells were isolated (phase image; A, right) and purified by FACS with anti-p75 antibody (B). Scale bar represents 50 μm.

(C) RT-PCR of purified p75^{+} Schwann cells. Highlighted genes (red dots) are late Schwann cell developmental and myelin markers that are not present in neural crest cells. See also Figure S1.

(D) Purified Schwann cells were infected with *M. leprae* (ML), fixed at day 7, and immunolabeled with anti-p75 (red) and anti-PGL-1 (iML in green) antibodies, counterstained with DAPI (blue). Insets: BrdU uptake (green; top) and antibody to phospho-histone H3 (Ser28) (green; bottom) double-labeled with PGL-1 antibody (red). Scale bars represent 50 μm.

(legend continued on next page)

order to successfully infect other tissues and transmit infection. In leprosy patients, disseminated ML could be seen in several tissues, including skeletal muscles and smooth muscles (Pearson et al., 1970; Job, 1989; Kaur et al., 1981; Scollard et al., 2006; Werneck et al., 1999). Also, the involvement of skeletal muscles in human leprosy is considered secondary due to peripheral neuropathy with the obvious peripheral-nerve innervations of skeletal muscles (Pearson et al., 1970; Werneck et al., 1999). However, it is unknown how initial colonization of ML in Schwann cells subsequently leads to the spread of infection to other tissues.

In this study, we show that leprosy bacteria trigger reprogramming of adult Schwann cells to a stage of progenitor/stem-like cells (pSLC) with migratory and immunomodulatory properties that promote bacterial dissemination. Reprogrammed cells facilitate bacterial spread by two distinct mechanisms—by direct differentiation to mesenchymal tissues, skeletal muscles, and smooth muscles and by contributing to form granuloma-like structures (GLS) that subsequently release bacteria-laden macrophages. Our findings present an unexpected link between cellular reprogramming and host-pathogen interaction and thus direct to potential new therapeutic strategies for combating infections with pathogenic bacteria.

RESULTS

Schwann Cells Derived from Adult Peripheral Nerves Undergo Reprogramming Events in Response to Intracellular ML

We recapitulated the colonization of ML and subsequent early molecular events in adult Schwann cells by infecting primary Schwann cells isolated from adult mouse peripheral nerves. We isolated Schwann cells from adult wild-type and Sox2-green fluorescent protein (GFP) transgenic mice and purified by fluorescence-activated cell sorting (FACS) with antibody to Schwann cell-surface marker p75 ^{NTR} or GFP expression under the control of Sox2 promoter, respectively (Figures 1A–1C, 2A, and 2B and Figures S1 and S3A available online). Single-cell-derived Schwann cells were generated from FACS-sorted cells and characterized extensively (Figure S1). All were positive for the markers for late Schwann cell development and myelination-associated genes (Figures 1C and S1). Most of these differentiation markers are not present in neural crest stem cells and do not appear until around the time of birth (Jessen and Mirsky, 2005; Finzsch et al., 2010). Therefore, they represent mature dedifferentiated Schwann cells. Moreover, karyotyping of these cells showed intact chromosome numbers and no evidence of translocation, suggesting their genomic stability (Figure S1).

As expected, these dedifferentiated adult Schwann cells are highly susceptible to ML infection with rapid bacterial engulfment with >90% efficiency (Figures 1D, 2Ac, and S1). We performed extensive genome-wide transcriptome profiling with Affymetrix mouse genechips and subsequent RT-PCR and quantitative PCR (qPCR) analyses. Strikingly, infected Schwann cells compared to uninfected/control Schwann cells, which were maintained under identical experimental conditions, showed upregulation of numerous genes of embryonic development, transcription, chromatin remodeling, cell signaling, chemokines, and cell division-cycle/DNA replication (Figures 1I and S2). The latter was consistent with a moderate increase of S phase cells in infected cultures; despite the presence of numerous intracellular ML (iML), infected cells showed BrdU uptake and phospho-histone H3 (S28) positive nuclei, which represent the S and mitotic phases of the cell cycle, respectively (Figure 1D, insets). Strikingly, ML infection was followed by the removal or export of Sox10 from Schwann cell nuclei (Figures 1E–1G). Whereas, similar to uninfected/control cells, infected Schwann cells that carry fewer iML maintained Sox10 exclusively in nuclei, high bacterial load invariably caused the removal of nuclear Sox10, which might affect the regulation of its key target Schwann cell genes, including myelin gene Mpz (Figures 1E–1G) (Finzsch et al., 2010; Jessen and Mirsky, 2005; Weider et al., 2012). Indeed, downregulation of myelin genes was found in infected Schwann cells over time (Figure 1H). Sox10 is a master regulator of Schwann cell homeostasis, identity, and myelin maintenance as well as differentiation, with nuclear Sox10 being required to recruit chromatin-remodeling complexes (Finzsch et al., 2010; Weider et al., 2012). Therefore, bacterial-induced removal of Sox10 from nuclei is likely to perturb normal Sox10-mediated transcriptional events. Together, these findings set the stage for a potential reprogramming or change in Schwann cell fate in response to iML.

Mesenchymal Transition and Induction of EMT-like Program in Adult Schwann Cells

The fate of iML-induced effects on Schwann cells was examined by gene-expression analyses over a 4 week period. Strikingly, only infected cells gradually "turn off" Schwann cell differentiation/myelination- and lineage-associated genes and "turn on" numerous developmental genes, comprising mostly the mesoderm development, including homeodomain/Hox, EMT, and neural crest-related genes (Figures 1H, 1I, and S2); at day 27 post-infection, most of the Schwann cell lineage and differentiation/myelination genes, but not negative regulators of myelination like Sox2 and c-Jun (Jessen and Mirsky, 2005), were downregulated (Figures 1H and S2), suggesting that iML gradually shuts down the Schwann cell differentiation program. Figure 1I shows the selected key developmental-regulated transcription factor (DRTF) genes (with known functions; Table S1).

A major tissue-remodeling program that is central to early mesoderm development during embryogenesis is EMT (Polyak and Weinberg, 2009). Interestingly, master regulators of EMT, Twist1 and 2, Snail2, and Msx2, which are capable of inducing

(E–G) Expression of nuclear Sox10 in control (E) and infected (F) Schwann cells at day 10 post-infection; antibodies to Sox10 (red) and PGL-1 (iML; green), counterstained with DAPI (blue) (F). Shown in (F) are selected representative Deltavision images from infected cultures with high (arrows) and low bacterial loads (arrowheads). (G) Quantification of nuclear Sox10 in control and infected Schwann cells with iML per cell. Scale bars represent 10 μm.

(H and I) Gene array analyses at days 14 and 27 post-infection. Schwann cell lineage/differentiation-associated genes (H) and development- and EMT-associated transcription factor (TF) genes (I) are shown as fold change in expression.

See also Figure S2 and Table S1.

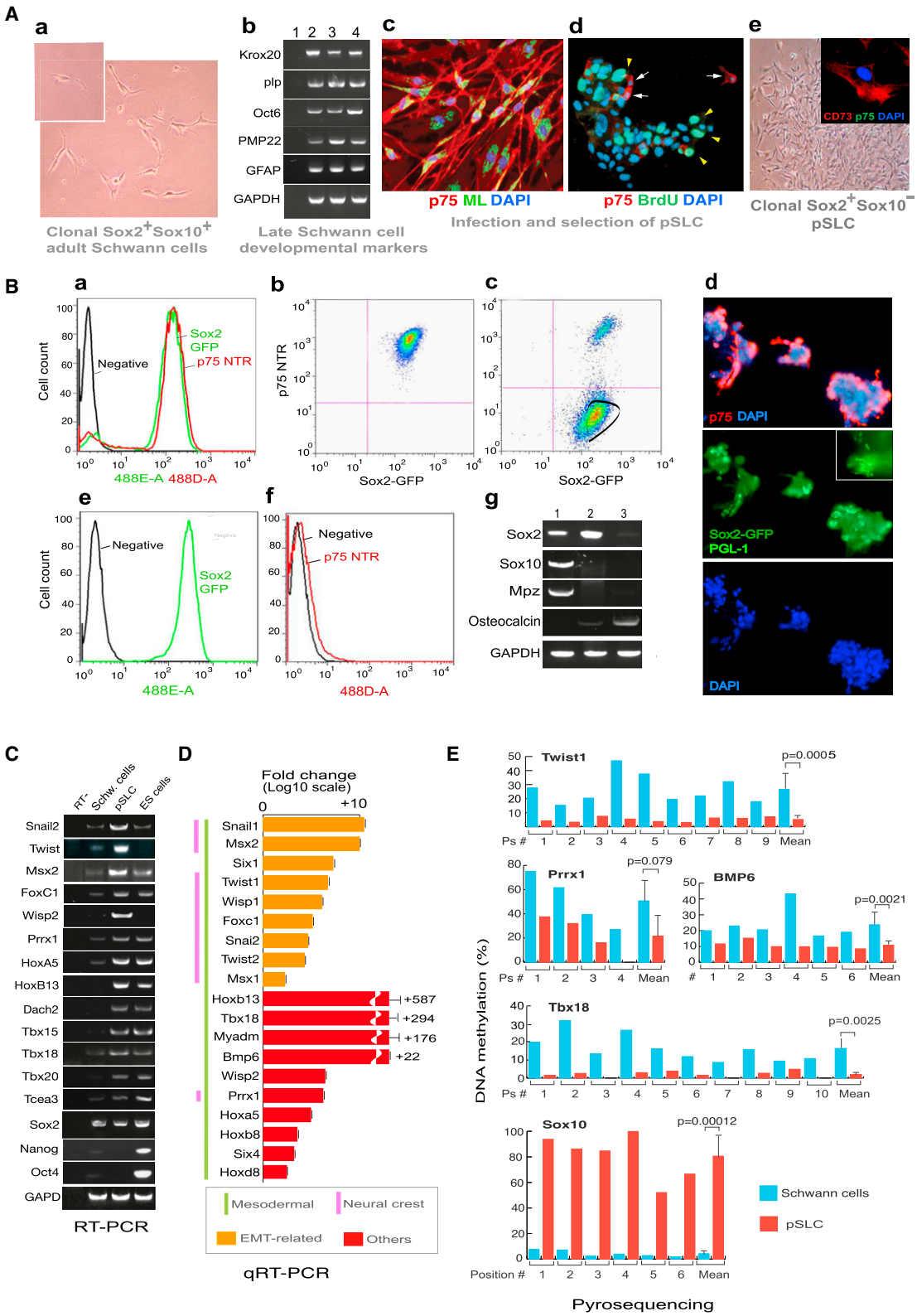

Figure 2. Induction of Mesenchymal Transition in Clonal Schwann Cells by ML Generates pSLC

(A) Phase image of single cell (inset)-derived Schwann cells from wild-type mice (a). (b) RT-PCR of p75^{+} FACS-sorted control Schwann cells from wild-type mice (lane 2), clonal Schwann cells from wild-type mice (lane 3), and clonal Schwann cells from Sox2-GFP mice (lane 4); lane 1, negative control (water only).

(legend continued on next page)

EMT in epithelial cells (Mani et al., 2008) (Table S1), were among the highly upregulated transcription factor (TF) genes in ML-infected Schwann cells (Figures 1I and S2). The observed cell-fate changes in Schwann cells are complex as infection involves upregulation of multiple developmental and functional genes (Figures 1H, 1I, and S2; Table S1), and these events are not associated with tumor-suppressor genes like p53 or Schwann cell tumor-associated gene NF1 (Figures S2A and S3A).

Our findings also suggest that reprogramming requires a high number of intracellular bacteria (>50 iML/cell with >90% infection efficiency) and a long-term incubation; we could not find any significant change in gene expression or the removal of nuclear Sox10 at a much lower rate of infection (<10 iML/cell; Figures 1E–1G). Shortage or lack of such optimum conditions appears to weaken or fail to induce transcriptional changes. For example, the observed changes in gene expression are highly significant with live ML, as compared to irradiated ML; bacterial components like PGL-1 did not show reprogramming events, despite their capacity to induce rapid demyelination upon their extracellular binding to myelinated Schwann cells (Rambukkana et al., 2002). This appears to be due to high invasion capacity of live ML and thus the long-term exposure of Schwann cells to a high number of iML. In addition, incubation of Schwann cells with other mycobacteria like *Mycobacterium smegmatis* did not lead to reprogramming (data not shown).

Bacterially Reprogrammed Schwann Cells Exhibit Properties Similar to pSLC

To isolate reprogrammed cells from the infected cell population, we transferred clonal-infected Schwann cells to mesenchymal stem cell medium (Mscm), which is selective for mesenchymal stem cells (MSC) from bone marrow cells (Li et al., 2009). In Mscm, only reprogrammed Schwann cells showed a high proliferation index as demonstrated by BrdU uptake (Figure 2Ad); >90% of these BrdU$^+$ cells were negative for Schwann cell lineage markers p75 and Sox10 as well as other mature phenotypes (Figure 2A). We used this property to select a p75$^-$ population by FACS sorting. Analyses of these p75$^-$ cells by microarrays, RT-PCR, qPCR, immunofluorescence (IF), and FACS revealed the loss of all Schwann cell lineage/myelin-specific markers and acquisition of various mesodermal and neural crest markers (Figures 2C, 2D, S3A, and S3B). Thus, we concluded that iML converted Sox2$^+$/p75$^+$/Sox10$^+$ Schwann cells to Sox2$^+$/p75$^-$/Sox10$^-$ reprogrammed cells with loss of Schwann cell markers (Figures 2B and S3A), which we referred to as pSLC because of their stem cell characteristics (see below). Further characterization revealed the expression of CD73, CD44, Sca-1, and Cd29 MSC markers but the absence of hematopoietic markers CD45, CD34, and c-kit (Figure S3H). pSLC also acquired highly migratory properties as evident by their migration through connective tissues when administered into injured muscles (Figures S3F and S3G).

Reprogramming Removes Schwann Cell Lineage/Myelin Regulator Sox10 and Maintains Stem Cell Marker Sox2

Conversion of parent Schwann cells to pSLC led to the loss of Schwann cell master regulator Sox10 but maintained Sox2. To track Sox2 expression during reprogramming, we generated clonal Schwann cells isolated from adult Sox2-GFP mice (Eminli et al., 2008). Clonal cells in Schwann cell media maintained both Sox10 and other mature Schwann cell markers, whereas infected cells lost Sox10 and other Schwann cell markers and subsequently changed into pSLC when maintained in Mscm (Figures 2A and 2B). Infected Schwann cells continued to maintain GFP (Sox2) expression but upon reprogramming lost expression of p75, Sox10, and other mature markers (Figures 2Ba–2Bd). When pSLC were maintained in Mscm, clusters of infected GFP$^+$ cells with both p75$^-$ and p75$^+$ were frequently observed (Figure 2Bd). When p75$^-$ reprogrammed cells in Mscm were isolated by FACS sorting, they continued to express GFP (Sox2) despite the loss of lineage/mature Schwann cell markers (Figures 2Bc–2Bg). However, GFP/Sox2 expression disappeared when pSLC were subjected to bone differentiation (Pittenger et al., 1999), which in contrast upregulated bone marker osteocalcin (Figures 2Bg and 3C), further underscoring stem cell characteristics of pSLC. Tracking the GFP expression from parent GFP$^+$/Sox2$^+$/p75$^+$/Sox10$^+$ Schwann cells to GFP$^+$/Sox2$^+$/p75$^-$/Sox10$^-$ pSLC at the clonal level, we confirmed that pSLC are derived from Schwann cells but not from any progenitor cell type within the Schwann cell preparation.

Reprogramming Schwann Cells to pSLC Accompanies Epigenetic Changes

We next examined whether this change in cell fate is epigenetically regulated. We analyzed DNA methylation at 5 methylcytosine in cytosine guanine dinucleotide (CpG) in the promoter regions of selected genes that are expressed and repressed in pSLC as compared to parent Schwann cells. Methylation status was assessed by bisulfite pyrosequencing, which allows quantitative determination of the extent of methylation of each cytosine

(c) Infected clonal wild-type Schwann cells at day 7 (PGL-1$^+$ML, green; p75$^+$ Schwann cells, red). (d) BrdU uptake (green arrowheads) of day 27-infected Schwann cells maintained in mesenchymal stem cell media (Mscm); anti-p75 antibody in red (arrows), and nuclei (DAPI) in blue. (e) Phase image of p75$^-$ FACS-sorted cells that express CD73 (e-inset). Magnification 20×; Inset (e): 40−.

(B) FACS analysis of GFP$^+$(Sox2$^+$)/p75$^+$ Schwann cells isolated from adult Sox2-GFP mice (a). Clonal GFP$^+$/p75$^+$ cells derived from FACS-sorted Schwann cells (b) were infected with ML for 4 weeks (also see Figure S1M) and transferred to Mscm, and Sox2$^+$/p75$^-$ population was gated for FACS (c). (d) IF analysis of aggregated infected cells maintained in Mscm before FACS; p75$^+$ (red) and DAPI (blue). Inset shows PGL-1$^+$ ML as green rods. (e and f) FACS analysis of sorted cells showing GFP$^+$/Sox2$^+$ (e) and p75$^-$ (f) cells, which are referred to as pSLC. (g) RT-PCR of control Schwann cells (lane 1), pSLC (lane 2), and pSLC in bone differentiation media (lane 3). Magnification (d): 10×.

(C) RT-PCR of embryonic/developmental marker genes in pSLC as compared to control Schwann cells and mouse ESCs. See also Figure S3.

(D) qPCR for differential expression of selected embryonic/developmental marker genes in pSLC relative to control Schwann cells. Data are mean ± standard error of the mean (SEM) from three samples.

(E) Cell-fate change of Schwann cells to pSLC accompanies changes in DNA methylation statuses of promoter regions of key developmental/EMT and Schwann cell-lineage genes as analyzed by pyrosequencing.

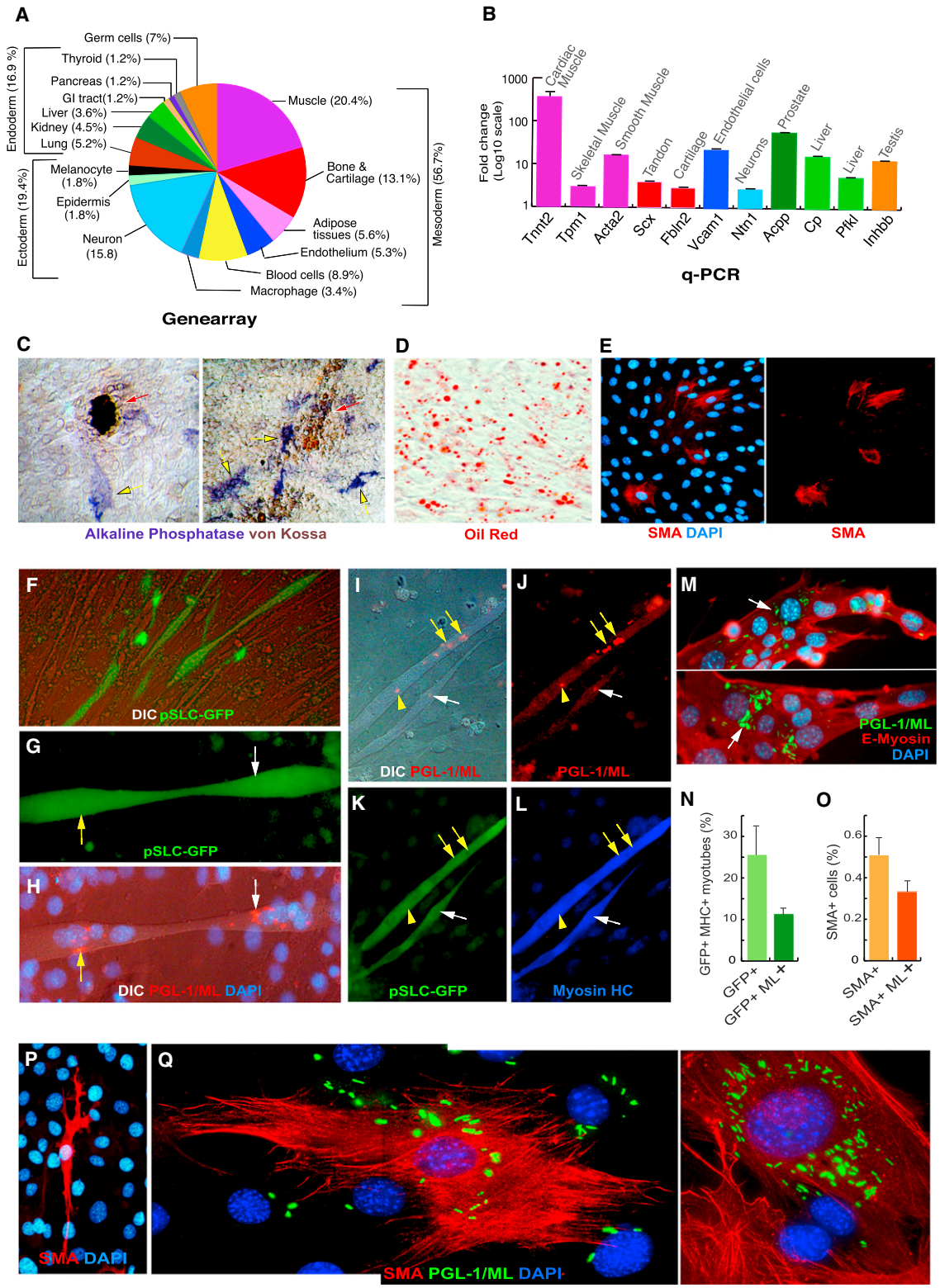

Figure 3. Broader Developmental Potential of Reprogrammed pSLC Promotes Bacterial Spread to Mesenchymal Tissues by Direct Differentiation

(A and B) Expression of tissue-specific gene clusters in pSLC as compared to control Schwann cells as analyzed by gene arrays (A). qPCR of some of the selected tissue-specific genes in pSLC. Data are mean ± SEM from two samples.

(legend continued on next page)

in a given DNA sequence (Extended Experimental Procedures and Data S1). We found that most CpG sequences in promoter regions of mesodermal/EMT genes, Twist1, Prrx1, Tbx18, and Bmp6, are significantly less methylated in pSLC as compared to Schwann cells (Figure 2E), suggesting that the epigenetic statuses of these genes were reprogrammed from a transcriptionally repressed state to an active state in pSLC. In contrast, the extent of methylation of the CpGs in Sox10 is significantly higher in pSLC and was strongly demethylated in Schwann cells. This correlates directly with loss of Sox10 expression in pSLC (Figures 2Bg and S3A). These findings suggest that reprogramming causes significant epigenetic changes in some of the key regulatory genes.

Differentiation Potential of Reprogrammed Schwann Cells to Mesenchymal Tissues

We analyzed gene arrays to assess the ability of pSLC to differentiate into different tissue types in Mscm (Figure 3A). Of the total tissue-specific genes, 56% of the transcripts accounted for mesoderm-related targets. qPCR of selected such genes confirmed these findings (Figure 3B). Consistent with these findings, pSLC differentiated into typical mesenchymal tissues under various well-established differentiation protocols. Under bone differentiation conditions, pSLC showed increased alkaline phosphatase activity and mineral deposition (Figures 3C and 2Ag); in adipocyte differentiation media, pSLC produced Oil Red O dye-positive lipid droplets that are characteristic of mature adipocytes (Figure 3D) (Pittenger et al., 1999). Based on the muscle-specific gene-expression patterns (Figures 3A, 3B, and S3), we also tested the potential of pSLC to differentiate into muscle lineage. Whereas pSLC spontaneously differentiated into SMA^+ smooth muscle-like cells (Figure 3E), coculturing pSLC with C2C12 myoblasts (Shi et al., 2004) contributed to myotube formation (Figure 3F). However, ML-induced reprogramming does not cause Schwann cells to acquire tumor formation capacity, as pSLC did not form teratomas or any kind of tumor formation in SCID mice (data not shown).

Reprogrammed Schwann Cells with Stem Cell-like Properties Promote Dissemination of Infection to Skeletal Muscles and Smooth Muscles by Direct Differentiation

We hypothesized that pSLC promote the transmission of ML into mesenchymal tissues by direct differentiation. As skeletal and smooth muscle tissues are known to harbor ML in leprosy patients, we used mouse models to test this hypothesis directly in vitro and in vivo (Gupta et al., 1975; Kaur et al., 1981; Pearson et al., 1970; Werneck et al., 1999).

Bacterial Dissemination by Direct Differentiation In Vitro

To determine whether ML spread to myotubes in a skeletal muscle-like microenvironment in vitro, we cocultured infected pSLC with C2C12 myoblasts (Shi et al., 2004). For these experiments we reinfected pSLC with ML in order to maintain bacterial load. Also, to track the contribution of pSLC, we introduced a lentivirus-based CopGFP reporter gene into clonal pSLC derived from wild-type Schwann cells. Stably expressed GFP^+ cells were isolated by FACS. When infected GFP^+ pSLC were cocultured with C2C12 myoblasts, pSLC fused with myoblasts and contributed to GFP^+ myotube formation (Figures 3F and 3G). This process accompanied the passive transmission of iML from GFP^+ pSLC to GFP^+ myotubes (Figures 3G and 3H). Immunolabeling with antibodies to PGL-1 (ML) and myosin heavy chain (myosin HC) confirmed the transmitted iML in GFP^+ multinucleated myotubes (Figures 3G and 3H) that are also positive for myosin HC (Figures 3I–3L). Antibody to E-myosin labeled the early stage of multinucleated myotubes with transmitted iML, and GFP^+ myotubes harboring iML clearly showed a passive bacterial transmission from reprogrammed pSLC following differentiation (Figures 3M and 3N).

We next tested the spread of ML to smooth muscle-like cells from infected pSLC. When pSLC were maintained in Mscm for several passages, ~0.5% of pSLC spontaneously differentiated into SMA^+ smooth muscle-like cells (Figure 3P). This propensity of pSLC allowed direct ML transfer from infected SMA^-pSLC to SMA^+ cells with a clear actin filament network that can easily be distinguished from undifferentiated pSLC (Figures 3P and 3Q).

Bacterial Dissemination by Direct Differentiation In Vivo

To further validate the in vitro findings, we used a widely used cardiotoxin-induced skeletal-muscle injury model, wherein damaged muscle fibers are replaced spontaneously by regenerated muscles in the presence of an anti-inflammatory microenvironment (Chargé and Rudnicki, 2004; Tidball and Villalta, 2010). We used nude mice, as they lack T cells and produce a relatively less complex inflammatory microenvironment comprising predominantly macrophages. Our rationale was that pSLC, which express muscle-development and differentiation genes similar to muscle progenitors (Figures 3 and S3), would contribute to myotube formation under the physiological conditions of an injury-induced regenerating microenvironment (Chargé and Rudnicki, 2004). Such conditions somewhat mimic the ML

(C–F) Differentiation potential of pSLC into various mesenchymal tissues. (C) Bone differentiation as analyzed by von Kossa staining (mineral/calcium deposition in brown; red arrows) and the expression of alkaline phosphatase activity (in blue; yellow arrows) (see also Figure 2Bg). (D) Adipocyte differentiation media produced mature adipocyte-like cells as detected by Oil red staining. (E) pSLC spontaneously differentiate into SMA^+ smooth muscle-like cells in culture. (F) Coculture of GFP^+ pSLC with C2C12 myoblasts contributed to GFP^+ myotube formation; shown is a live fluorescence/DIC image. Magnifications: 20×.

(G–N) pSLC passively transfer infection to myotubes following differentiation. Infected GFP^+ pSLC (green) transfer ML to GFP^+ myotubes upon differentiation under the influence of C2C12 myoblasts. Multinucleated GFP^+ myotubes (G and H) show the acquisition of ML (white and yellow arrows) as detected by anti-PGL-1 antibody (red) counterstained with DAPI and visualized under fluorescence/DIC (H). These ML^+ GFP^+ myotubers were also positive for myosin HC (I–L). Antibody to E-myosin detected early stages of multinucleated myotubes that carry numerous iML (M). (N) Quantification of GFP^+ myotubes with and without ML. Magnifications: (G, H, and M): 40×; (I–L): 20×.

(O–Q) ML-infected pSLC spontaneously differentiate into SMA^+ smooth muscle-like cells as detected by antibodies to PGL-1 (green) and SMA (red) counterstained with DAPI (blue) (P and Q). (O) Quantification of SMA^+ cells with and without ML. Magnification: (P) 40×; (Q) 60×.

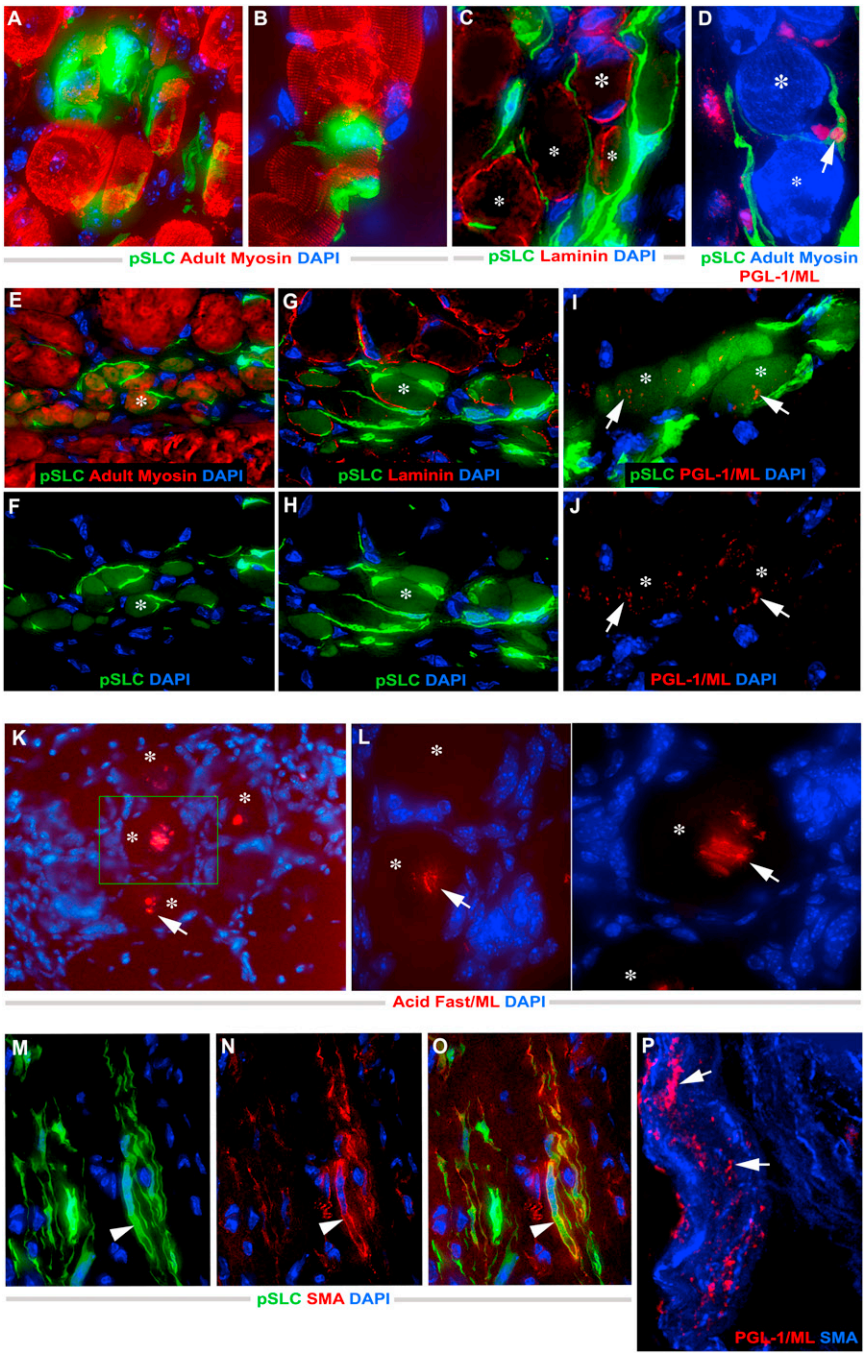

Figure 4. Redifferentiation of Reprogrammed pSLC Contributes to Passive Bacterial Transfer to Skeletal Muscles and Smooth Muscles In Vivo

(A–D) Transverse frozen sections of TA muscles injected with ML-infected GFP$^+$ pSLC after 10 days. Deltavision images showed GFP$^+$ pSLC (green) either fused with myofibers (A and B) or migrating in between muscle fibers (C and D). Antibodies to adult myosin detected muscle fibers (red in A and B and blue in D), and laminin demarcated individual muscle fibers (red in C). Antibodies to PGL-1 detected ML (in red; arrow) associated closely with muscle fibers (D). Asterisks in all figures denote individual myofibers. Magnifications: 60×.

(E–J) Infected GFP$^+$ pSLC were incorporated into regenerating muscles at 3 weeks post-injection. GFP$^+$ myofibers are positive for adult myosin (E and F) and are demarcated by laminin (G and H). pSLC incorporation passively transmitted ML to myofibers as detected by PGL-1$^+$ ML (red; arrows) in GFP$^+$ myofibers (I and J). Magnifications (Deltavision images): 40×.

(K and L) Bacterial presence within the skeletal muscle fibers (asterisks) was confirmed by acid-fast mycobacterial staining (red). Arrows show clumps of rod-shaped ML in several individual muscle fibers. Magnifications: 60×.

(M–P) Administered infected GFP$^+$ pSLC differentiate into SMA$^+$ smooth muscles in the dermal area. Antibody to SMA (red) colocalizes with differentiated GFP$^+$pSLC (green; arrowheads); merged image is shown in (O). Magnifications: (M–O) 40×. (P) Higher magnification (100×) showed the PGL$^+$ML (red; arrows) within SMA$^+$ smooth muscles (blue) near dermal vessels.

infection-associated inflammation in muscles and thus commensurate with the muscle pathology documented in the lepromatous form of leprosy in patients with high bacterial load (Gupta et al., 1975; Werneck et al., 1999).

We first injected cardiotoxin into the tibialis anterior (TA) muscles of nude mice, and the muscle injury, inflammation, and repair process were confirmed by histological studies and immunolabeling (data not shown). GFP$^+$ pSLC containing ML were then injected into preinjured TA muscles, and their distribution was examined at different time intervals. Antibody staining to adult myosin clearly showed the intimate interaction and early fusion process of ML-laden GFP$^+$ cells around the muscle fibers at the injury site after day 10 (Figures 4A–4D). The engrafted GFP$^+$ pSLC were detected within muscle milieu at days 14 and 21 either as fused to resident regenerating fibers or fully integrated into smaller diameter myofibers that express adult myosin and are demarcated by laminin in the basal lamina (Figures 4E–4H). Anti-PGL-1 antibody staining that specifically identifies ML (Ng et al., 2000) confirmed the bacterial presence within fully integrated GFP$^+$ myofibers (Figures 4I and 4J). Specific acid-fast mycobacterial staining further confirmed rod-shaped ML within myofibers (Figures 4K and 4L). In contrast to pSLC, injection of nonreprogrammed infected GFP$^+$ Schwann cells (infection only for 2 days) to injured TA muscles failed to transmit infection to regenerating muscle fibers (data not shown).

Similarly, we also found that administered infected GFP$^+$ pSLC can differentiate into SMA$^+$ smooth muscles (or myofibroblasts),

and ML can be detected within SMA$^+$ smooth muscles in the dermal area of muscle-skin interphase and associated blood vessels (Figures 4M–4P). In contrast, infected GFP$^+$ Schwann cells (nonreprogrammed cells infected for 2 days only) neither differentiated into smooth muscles nor contributed to transferring infection to SMA$^+$ cells (data not shown). Together, these results suggest that under the influence of injury and inflammatory tissue microenvironment, infected pSLC could elaborate their migratory capacity and differentiate into myofibers or smooth muscles and passively transmit ML to these tissues that are favorable for sequestration of infection.

Reprogrammed pSLC Acquire Immunomodulatory Properties

We examined whether reprogrammed pSLC also secrete immunomodulatory factors in a way similar to that of MSCs. To test this, we first used mouse chemokine/cytokine protein arrays to analyze proteins released into serum/supplement-free conditioned media (CM) from pSLC. Figure 5A shows the quantitative analysis of differentially expressed soluble proteins released by pSLC. Strikingly, pSLC produced a range of chemokines, cytokines, growth/survival factors, soluble adhesion receptors, and tissue-remodeling factors to varying degrees (Figures 5A and S4). These findings also validate the MSC-like functional properties of pSLC because almost all chemokines/cytokines that are known to be produced by MSC are also released by pSLC (Figure 5A) (Hoogduijn et al., 2010; Klopp et al., 2011). Although a fewer number of these proteins are also released by control/uninfected Schwann cells, the fold increase of their expression is several fold higher in pSLC (Figures 5A and S4), suggesting a greater potential of pSLC to participate in multiple immunomodulatory functions. Interestingly, once reprogrammed, pSLC continued to secrete soluble factors regardless of bacterial presence, as complete removal of ML from pSLC (with no detectable ML genomic DNA) continued to produce almost the same soluble proteins (Figures 5A, inset and S4).

pSLC-Derived Soluble Factors Mediate Macrophage Survival and Migration

We next examined the functional effects of pSLC-derived immunomodulatory factors on tissue macrophages. As a source, we used freshly isolated mouse peritoneal macrophages, which comprised >85% F4/80$^+$ and ~100% CD68$^+$ macrophages. When incubated with pSLC-CM alone, both F4/80$^+$ and CD68$^+$ macrophages were maintained >14 days, whereas the majority of macrophages in medium alone did not survive or lifted off early in cultures (Figure 5B). Macrophages maintained in pSLC-CM showed a firm attachment and elongated morphology with strong F4/80 expression, suggesting possible maturation of macrophages in pSLC-CM. pSLC-CM also influenced increased survival of macrophages with minimum apoptosis (Figure 5C). However, pSLC-CM did not increase S phase cells significantly (data not shown).

Consistent with the chemokine/cytokine production, pSLC-CM attracted a significant number of macrophages when a cell migration assay was performed with the Trans-well system (Figures 5D–5F). Migration capacity was further increased in the presence of live pSLC, implying that freshly secreted pSLC factors attracted a higher number of macrophages (Figures 5E and 5F). Although pSLC-CM-induced macrophage migration was slightly decreased (<10%) in the presence of a standard dose (200–1000 ng) of broader CC-chemokine inhibitor, CCI (recombinant viral CCI-Fc chimera), which has shown to be effective in other studies (Buatois et al., 2010), a high dose of nontoxic concentrations of CCI (5000 ng) was required to produce a significant inhibition of migration (Figure 5G). Because pSLC produce an array of soluble proteins (Figures 5A and S4), our data suggest that a collective effect of immune factors, but not CC-chemokine alone, is required to exert effective macrophage chemotactic ability.

Reprogrammed pSLC Promote Bacterial Dissemination via Macrophages In Vivo

We reasoned that a nude-mouse muscle-injury model with a predominantly macrophage-containing inflammatory microenvironment would be useful to directly test whether pSLC promote bacterial dissemination via macrophages. To ensure that all injected pSLC express GFP and all bacteria are inside the cells, strongly positive GFP$^+$ pSLC were FACS sorted and reinfected with ML 2 days before cell injection to the preinjured TA muscles. Analyzing the fate of pSLC and iML at weeks 1, 2, and 3 post-injection revealed that almost all GFP$^+$ cells migrate further away from the site of injection after 1 week and continue to spread over time along the interstitial connective tissues in the perimysium and to the skeletal muscle-dermal interphase (SkMDIP) at week 3 post-injection (Figures 6A, S5, and S6). Strikingly, iML were no longer confined to pSLC as most of iML were detected within recipient non-GFP cells (Figures 6Aa, 6Ab, 6Ah, and 6Aj). These data indicate that iML were efficiently transferred from donor GFP$^+$ pSLC to GFP$^-$ recipient tissue cells in vivo. Both anti-PGL-1 antibody and acid-fast mycobacterial staining confirmed these findings (Figures 6Aj and S5). These ML$^+$ GFP$^-$ cells were identified as endogenous macrophages as >90% of them were positive for macrophage markers F4/80, CD11b, CD68, and CD206 (Figures 6Ac–6Aj and S5).

Inflammatory conditions in cardiotoxin-induced TA muscles are known to bring a sequential appearance of macrophage subpopulations, initially with CD68$^+$ M1 subtype peaks at week 2 followed by a high CD163/CD206 M2 population that overlaps within the M1 population at week 2–3 post-injury (Tidball and Villalta, 2010). These established conditions allowed us to correlate GFP$^+$ pSLC distribution with infiltrated macrophage subtypes in injured muscles in a timely manner. Indeed, our findings with serial tissue sections from infected GFP$^+$ pSLC engrafted mice at week 3 post-infection showed that CD68$^+$, CD163$^+$, CD206$^+$, or F4/80$^+$ cells in the interstitial tissues were codistributed with GFP$^+$ pSLC. Double immunolabeling with an antibody to PGL-1 and macrophage markers confirmed iML within these macrophages (Figures 6Aj, S5K, and S5L). Once ML transferred from pSLC to macrophages, they appeared to transmit infection to uninfected macrophages and thus facilitate ML spread via these tissue macrophages along the connective tissues in between muscle fibers and SkMDIP. Figures 6Aa, S5, and S6 clearly show examples illustrating the presence of iML within numerous non-GFP recipient cells along the perimysium/connective tissues and SkMDIP. Analysis of serial tissue sections

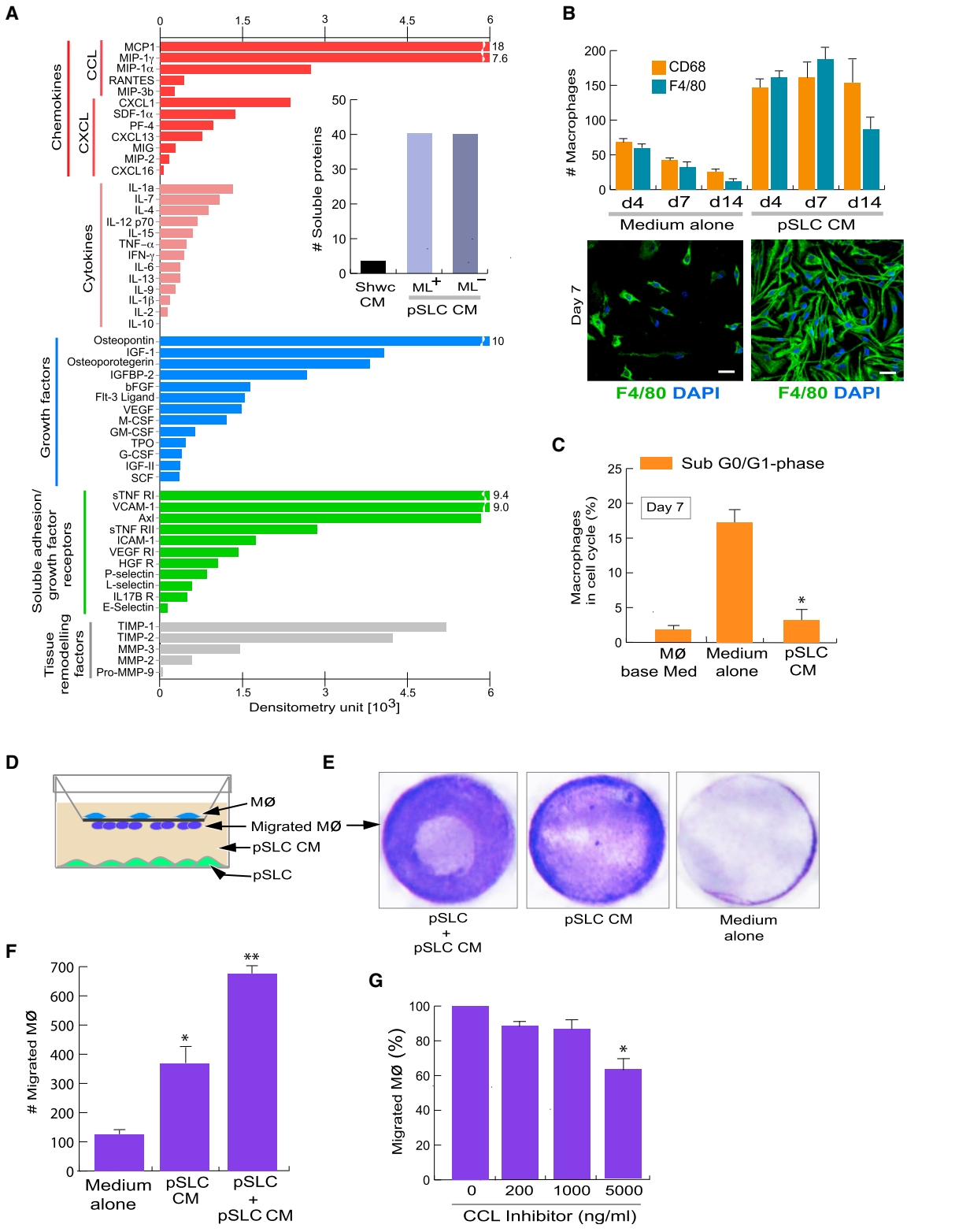

Figure 5. Reprogrammed pSLC Secrete Immune/Growth Factors that Promote Macrophage Survival and Migration

(A) Protein arrays of CM from infected pSLC showing the secretion of indicated classes of soluble factors. Relative levels of released proteins were detected by dot blot chemiluminescence and are presented as mean values from two arrays. Inset shows the number of detectable soluble factors released from CM from control Schwann cells (Schwc-CM) and pSLC (pSLC-CM) with and without iML (+/−ML). Also see Figure S4.

(legend continued on next page)

strongly suggests ML transfer from pSLC to both M1 and M2 macrophages (Figures 6 and S5).

pSLC Contribute to Granuloma-like Formation In Vivo: Role in Bacterial Dissemination

Strikingly, infected pSLC that had migrated to the loosely associated connective tissue areas within SkMDIP formed organized aggregates together with macrophages (Figures 6B and S6). These organized aggregates resemble typical granulomas seen in mycobacterial infections, both in murine models and humans (Flynn and Chan, 2001; Bold and Ernst, 2009; Modlin and Rea, 1988). Analyzing the cellular distribution of these GLS revealed that pSLC contribute to a major cellular mass highly organized into a spiral form of GFP^+ cells and interposed between infiltrated macrophages in both the core area and the periphery of GLS (Figure 6B). Interestingly, a distinct distribution of macrophage subpopulation was observed within these GLS: the exteriors of the GLS are strongly positive for F4/80 ($F4/80^{+high}$) and CD206 populations, whereas the core areas are weakly positive for F4/80 ($F4/80^{+low}$) but strongly positive for $CD68^+$ cells with tightly packed multinucleated macrophages (Figures 6Ba and S7). This phenotypic distribution of macrophages with $F4/80^{+high}/CD206^{+high}$ and $F4/80^{+low}/CD68^{+high}$ corresponds to M1 and M2 subtypes, respectively (Figures 6B, S6, and S7) (Mosser and Edwards, 2008). Anti-PGL-1 and Fite's staining (modified acid-fast mycobacterial staining) in serial sections clearly showed that macrophages in both core and periphery of GLS harbor large numbers of iML (Figures 6B, S5, and S6). In contrast, we were unable to detect such GLS when infected GFP^+ Schwann cells were administered under similar experimental conditions.

Release of ML-laden Macrophages from the Granulomas

We found a significant shift in distribution of macrophages when analyzed across granuloma-containing tissues within SkMDIP. Figures 6B and 6C illustrate the distribution of pSLC and macrophages and their bacterial contents within the GLS in serial sections taken from 250–300 μm apart tissue areas. In one end of the GLS-bearing tissues, $CD68^+$ cells with a high number of iML were organized into the core area surrounded by GFP^+ pSLC and bacterial laden $F4/80^{+high}/CD206^{+high}$ macrophages in the exterior, whereas in the other end, both $CD68^+$ and $CD206^+$ macrophages were found migrating out of the tapered aggregates of pSLC carrying iML with them (Figures 6B, 6C, and S6). These data collectively suggest not only the transfer of ML from pSLC to macrophages but also the migration of these bacterial-laden macrophages from the organized GLS.

In Vitro Granuloma-like Formation by pSLC and Macrophages

Next we developed an in vitro model of GLS. We found that pSLC tend to form aggregates at high density, and no leaked bacteria were found outside the aggregates (Figure 7A). Real-time microscopy revealed that uninfected macrophages migrated into infected GFP^+ pSLC aggregates when peritoneal macrophages were added (Figure 7B). Most of these macrophages reached the core area of the GLS as early as 6 hr and 18 hr and acquired ML from pSLC; bacterial transfer from some infected pSLC to macrophages was also observed adjacent to the GLS (Figures 7B). Some macrophages were also found to contain GFP^+ pSLC cell debris with the bacteria in them, suggesting the phagocytosis of dead or apoptotic GFP^+ pSLC by macrophages (Figure 7B). However, only ~0.04% of TUNEL-positive cells were detected in these cell aggregates. Over time, an increasing number of macrophages continued to migrate and form larger GLS, and at this point, most of the ML were transferred to macrophages (Figure 7C). These organized GLS then gradually started to disintegrate and subsequently release ML-laden macrophages (Figure 7D). Quantification of bacterial transfer from pSLC to macrophages showed an effective transmission of infection to macrophages over time (Figure 7E). These findings suggest that chemoattractants released from pSLC aggregates may have provided the right signals for macrophage migration and GLS formation. Further studies on dissection of regulatory signaling pathways involved may establish new links between host cell reprogramming and innate phase immune responses during infection.

DISCUSSION

In this study, we provide evidence that leprosy bacteria perturb dynamic mechanisms that normally preserve the lineage commitment of adult Schwann cells and hence change the Schwann cell fate to pSLC with mesenchymal characteristics that promote bacterial dissemination. The findings describe an unexpected but natural exploitation of adult Schwann cell plasticity by ML during infection. Once invaded, ML gradually "turn off" Schwann cell lineage/differentiation-associated genes/TFs and "turn on" numerous embryonic/developmental genes and TFs of mesoderm and neural crest. Such alterations in gene expression are likely to disrupt the stoichiometry of transcriptional regulators, leading to reprogramming of infected cell nuclei.

Of particular interest is the induction of TFs of the homeodomain/Hox family and EMT in Schwann cells in response to ML. It is known that the fate of somatic cells can be altered by forced expressions of both Hox and EMT genes (Mani et al., 2008).

(B) Soluble factors secreted by pSLC promote macrophage survival. Quantification of adherent $F4/80^+$ and $CD68^+$ macrophages maintained in pSLC-CM and media alone for up to 14 days is shown (B, top panel). IF of adherent $F4/80^+$ macrophages in the presence of pSLC-CM (right) and media alone (left) at day 7 is also shown (B, bottom panel). Magnifications: 20×.

(C) Macrophages in indicated culture conditions in the sub G0/G1 cell-cycle phase that corresponds to apoptotic cells, as analyzed with propidium iodide. Data are presented as mean ± SEM from three experiments; *$p < 0.001$.

(D–G) pSLC secretory factors promote macrophage migration. (D) Schematic for the macrophage transwell migration assay in response to CM or media containing viable pSLC. (E) Crystal violet dye staining of migrated macrophages through the membrane under the influence of indicated conditions. (F) Quantification of migrated macrophages. (G) Effect of CC-chemokine inhibitor on macrophage migration in response to pSLC-CM. The data shown in (F) and (G) are presented as mean ± SEM from three experiments; *$p < 0.01$, **$p < 0.001$.

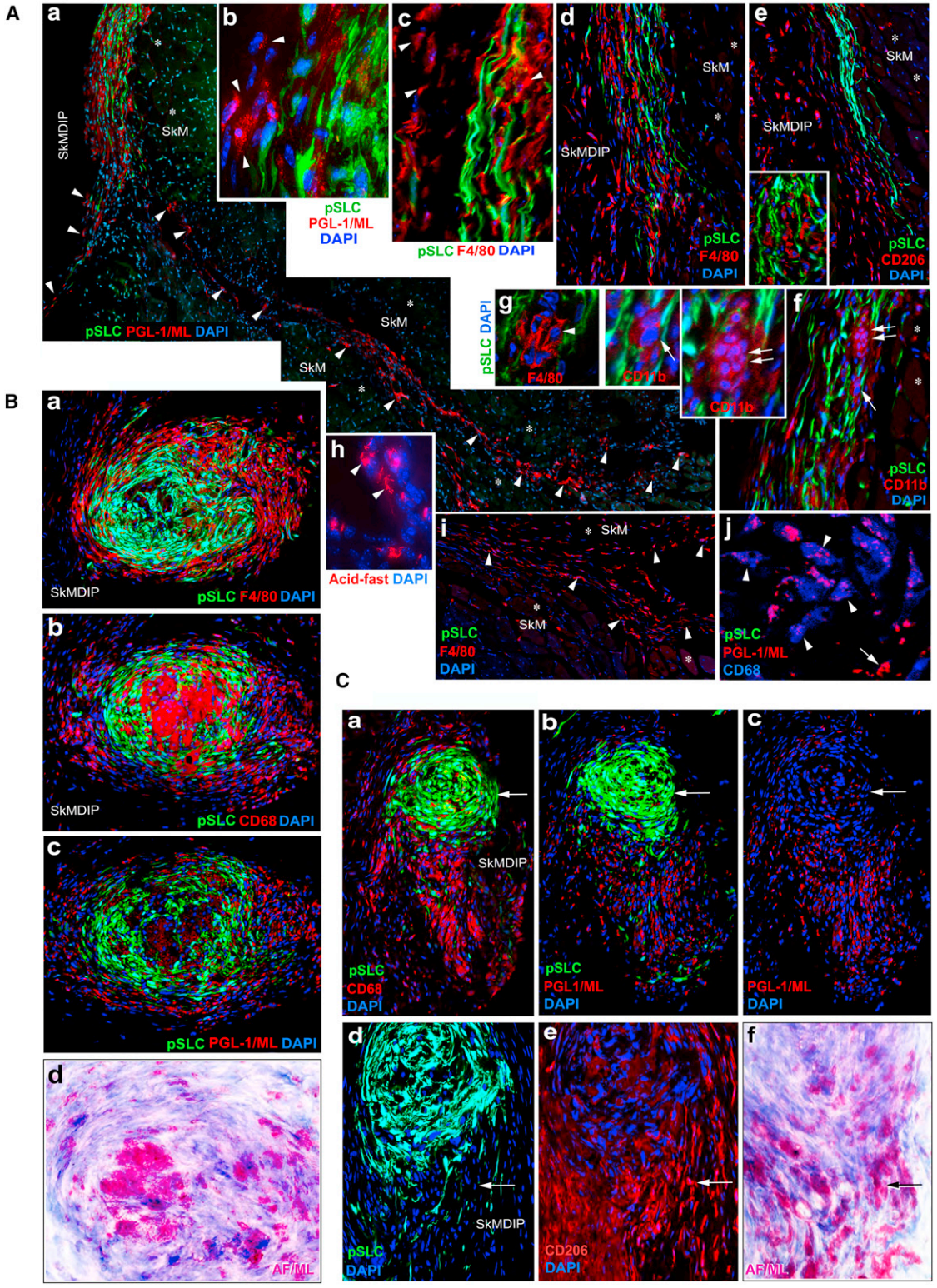

Figure 6. Reprogrammed pSLC Promote Bacterial Dissemination via Macrophages and Granuloma Formation In Vivo

(A) pSLC intimately associated with infiltrating macrophages and transferred infection effectively to recipient tissue cells in TA muscles. ML-infected GFP-pSLC were administered into preinjured TA muscles of athymic nude mice, and transverse sections at days 14 and 21 post-injection were labeled with antibodies to PGL-1 (ML in red; a and b) and various macrophage markers: F4/80 (c, g, and i), CD206 (e), CD11b (f), and CD68 (j). In (j), ML (red) were colocalized with CD68

(legend continued on next page)

ML-infected cells upregulated several Hox and key EMT-associated TFs, including the master regulators of EMT, Twist and Snail (Polyak and Weinberg, 2009; Mani et al., 2008). Demethylation of the promoter region of Twist1 in reprogrammed cells further suggests that the change in cell fate accompanies the change in epigenetic status. Reprogramming that follows the silencing of Sox10, the master regulator of Schwann cell lineage and differentiation/myelination (Finzsch et al., 2010; Jessen and Mirsky, 2005), directly correlates with significant DNA methylation of Sox10 in pSLC. On the other hand, no change in DNA methylation in the Sox2 promoter region (data not shown) suggests the continuous expression of Sox2 in both parent Schwann cells and pSLC. Thus, the silencing of Sox10 and maintaining or induction of Sox2 may be critical for Schwann cell reprogramming during infection.

In contrast to $Sox2^{+}/Sox10^{-}$ pSLC, nerve injury-induced dedifferentiated Schwann cells maintain $Sox2^{+}/Sox10^{+}$ and other Schwann cell markers (Le et al., 2005). Safeguarding the Schwann cell lineage markers, particularly Sox10, is critical for an effective differentiation towards myelination during the peripheral nerve regeneration process (Le et al., 2005; Finzsch et al., 2010). This phenotypic difference together with the acquisition of numerous mesoderm developmental genes distinguishes pSLC from nerve injury-induced dedifferentiated Schwann cells. On the other hand, our previous studies have shown that the initial interaction of extracellular ML with myelinated Schwann cells induces demyelination, which in turn generates similar dedifferentiated cells (Rambukkana et al., 1997, 1998, 2002; Tapinos et al., 2006). ML appear to use this demyelination strategy to generate dedifferentiated Schwann cells as they are highly susceptible to invasion and favorable for bacterial colonization (Rambukkana, 2010). In the present study, we mimicked such conditions by directly isolating dedifferentiated Schwann cells from adult mouse peripheral nerves and showed that, once invaded, iML reprogram these Schwann cells to pSLC. It remains to be determined which mechanisms or signaling are involved in this bacterial-driven cell reprogramming.

The important role of Erk1/2 MAPK signaling in inducing demyelination without immune responses or lesions was first demonstrated with leprosy bacteria as a model (Tapinos et al., 2006). This finding was recently confirmed with inducible Raf-kinase transgenic mice in which Erk1/2 activation in myelinated Schwann cells was shown to induce demyelination and inflammatory responses (Napoli et al., 2012). Interestingly, the latter activates p75, whereas reprogramming Schwann cells to pSLC results in the loss of p75 (Figure 2). Also, unlike Erk1/2-induced demyelination where transiently appearing inflammatory cells promote peripheral nerve regeneration, pSLC acquired sustainable secretion of numerous macrophage chemoattractants even after complete removal of ML. This capacity may facilitate continuous attraction of macrophages to pSLC in many tissues during the early dissemination process. Although ML use Erk1/2 signaling for Schwann cell manipulation (Tapinos and Rambukkana, 2005; Tapinos et al., 2006), Erk1/2 alone does not appear to contribute to reprogramming as the pharmacological inhibition of Erk1/2 did not abrogate the reprogramming events (data not shown). This further suggests that the activation of Erk1/2 alone does not cause Schwann cell reprogramming.

Although the lineage through which infected Schwann cells are converted to pSLC is not known, this change may have important benefits for a bacterium like ML that depends totally on host cell functions for survival (Cole et al., 2001). Conversion of Schwann cells to pSLC with mesenchymal characteristics sets the stage for ML to use the reprogrammed cells as a vehicle to spread the infection to distal tissues such as skeletal and smooth muscles. We propose two major mechanisms by which ML may use reprogrammed cells to promote bacterial dissemination (Figure 7H). First, ML take advantage of mesenchymal stem cell-like properties of pSLC to migrate and spontaneously differentiate into skeletal and smooth muscles under inflammatory conditions and thus passively transmit infection to these tissues. Second, using immunomodulatory properties of pSLC, ML may use reprogrammed cells to create a secondary niche by recruiting macrophages for further bacterial expansion and dissemination.

Importantly, our findings in vivo showed that pSLC contribute to macrophage granuloma formation, one of the pathologic hallmarks of mycobacterial infections in murine models and in patients with both leprosy and tuberculosis (Modlin and Rea, 1988; Flynn and Chan, 2001). Although mycobacterial granulomas are considered to be essential for containment of infection, recent studies in zebrafish have suggested that macrophage granulomas may also promote mycobacterial dissemination during early infection (Davis and Ramakrishnan, 2009). However, unlike other pathogenic mycobacteria, ML use adult Schwann cells as primary nonimmune tissue cells for initial colonization (Stoner, 1979). Once colonized, ML take full advantage of Schwann cell plasticity to convert infected cells to pSLC

(blue; arrowheads). Endogenous non-GFP tissue cells that have taken up ML are shown with arrowheads (a) and are predominantly comprised of infiltrated macrophages of M1 and M2 phenotypes (e, i, and j). ML localization is confirmed by acid-fast staining (red) in parallel sections (h). Insets in (e), (f), and (g) (arrows and arrowheads) show the formation of early smaller macrophage GLS. SkM: skeletal muscles (asterisks); SkMDIP: skeletal muscle-dermal interphase. Magnifications: (a, d, e, f, and l) 10×; (b, c, g, and h) 40×.

(B) pSLC contribute to the formation of typical macrophage GLS in SkMDIP. Migrated pSLC formed organized GLS with M2 and M1 macrophages that show distinct distribution and morphological features, as analyzed by antibodies to F4/80 (a) or CD206 (see also Figure S7) and CD68 (b), respectively. The distribution of ML (red) within GLS was localized in parallel sections with antibody to PGL-1 (c) and by Fite's staining (in purple), which detects mycobacteria in infected tissues (d; also see Figure S7). Note the strongly $F4/80^{+}$ cells in the periphery and fused and multinucleated $CD68^{+}$ cells in the core of GLS. Magnifications are 20×.

(C) Disintegration and release of bacterial-laden macrophages from granulomas. Sections distant from the granulomas (as in B) within the same tissues show disintegration of both CD68 (a) and CD206 (e) macrophages from tapered GFP^{+} pSLC aggregates (a–c) and the emigrating macrophages carrying large numbers of ML as detected by anti-PGL-1 (red; b and c) and Fite's staining (f). Arrows in the top and bottom panels show the pSLC with much fewer iML and high content of acid-$fast^{+}$ ML in migrating macrophages, respectively. Magnifications: (a–c) 10×; (d–f) 40×.

See also Figures S5, S6, and S7.

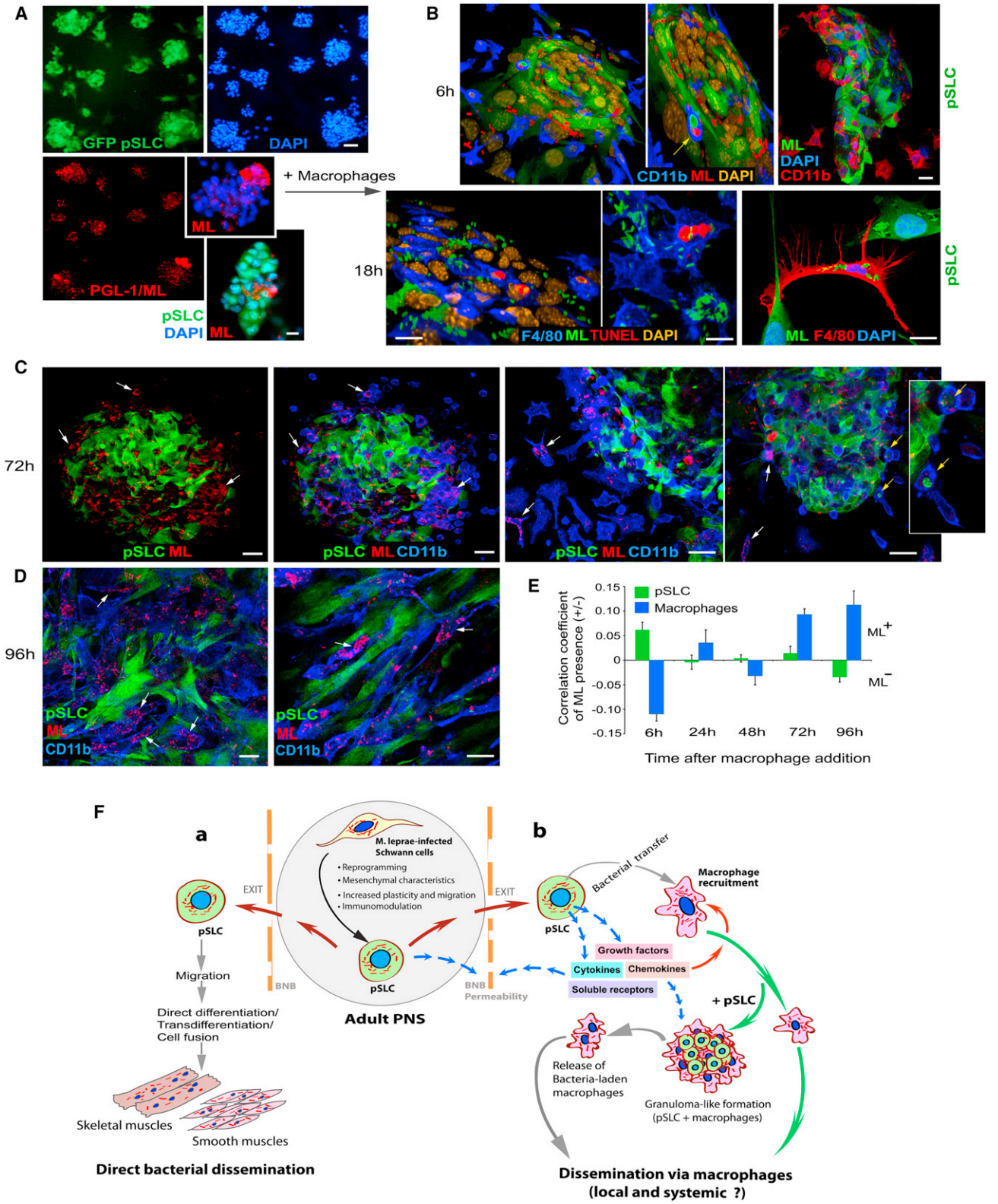

Figure 7. In Vitro Granuloma-like Formation with pSLC Recapitulates Bacterial Spread via Macrophages

(A) Infected GFP$^+$ pSLC form aggregates in culture (top panel) and ML confined strictly within the aggregates (bottom left) and form bacterial clusters (red; bottom insets), as detected by antibody to PGL-1 (red; bottom left), counterstained with DAPI (blue).

(legend continued on next page)

with the capacity to produce chemoattractants and trophic factors, which in turn promote macrophage recruitment, bacterial transfer, and survival of infected macrophages (Figures 5, 6, and 7H). Interestingly, some of the immune factors/chemokines released from pSLC are also known to foster granuloma formation (Qiu et al., 2001; Chiu et al., 2004). Collectively, these events may facilitate pSLC to recruit macrophages and contribute to form GLS. Our in vivo and in vitro analyses provide further evidence that ML-laden M1 and M2 macrophages in the granulomas contributed to spread the infection. Recent work showing that the viruses used for reprogramming skin fibroblasts to pluripotent stem cells (Takahashi and Yamanaka, 2006) can promote the efficiency of nuclear reprogramming via activation of common microbial-induced innate immune responses (Lee et al., 2012) conceptually supports our study. Finally, our findings may have far-reaching implications not only for host-pathogen interactions but also for understanding the basic biology of adult-tissue cell plasticity, reprogramming, and tissue regeneration.

EXPERIMENTAL PROCEDURES

Primary Adult Schwann Cell Cultures

Detailed experimental protocols for isolation and characterization of mouse primary Schwann cells are described in the Extended Experimental Procedures.

Infection with ML

Schwann cells were infected with ML according to our previous protocol (Ng et al., 2000; Extended Experimental Procedures). In vivo-grown ML derived from nude-mouse footpads were prepared as described previously (Truman and Krahenbuhl, 2001; Lahiri et al., 2010), and both viable and nonviable ML were provided by the Laboratory Research Branch of NHDP (Baton Rouge, LA, USA).

Mice

These studies employed 4- to 6-week-old young adult CD-1 (ICR) (strain code: 022) mice (Charles-River Laboratory), GFP mice that constitutively express eGFP (strain: C57BL/6-Tg [ACTB-EGFP] 1Osb/J, stock: 003291; Jackson lab [Bar Harbor, ME, USA]), 6- to 8-week-old CD-1/nude mice (Charles-River), and 4- to 6-week-old NOD-SCID mice (Jackson Lab). Sox2/GFP mice (Eminli et al., 2008) were kindly provided by R. Jaenisch (Whitehead Institute, MIT, Cambridge, MA, USA). Animals were maintained at the Rockefeller University and University of Edinburgh animal facilities according to institutionally approved protocols.

Flow Cytometry, Immunolabeling, Antibodies, and Microscopy

Flow cytometry, primary Schwann cell sorting, generation of clonal cells, immunolabeling with primary antibodies, and imaging (Confocal, Deltavision, and Time-lapse live-cell imaging) are described in the Extended Experimental Procedures. Antibodies to Sox10, ML PGL-1, and Oct6 were gifts from M. Wagner, A. Kolk, and D. Meijer respectively. A list of other antibodies used is available in Table S2.

Schwann Cell Infection with ML and Reprogramming Protocol

FACS-sorted p75$^+$ Schwann cells or clonal Schwann cells generated from wild-type mice or Sox2-GFP mice were infected with ML as described (Ng et al., 2000; Tapinos and Rambukkana, 2005). For the isolation of reprogrammed cells, infected cells were transferred to mesenchymal stem cell media that allowed the selection of a pSLC population based on the cell-fate change from p75$^+$/Sox10$^+$ cells to p75$^-$/Sox10$^-$. These cells were FACS sorted with p75 antibody and subjected to detailed characterization (Extended Experimental Procedures). pSLC were also transduced with CopGFP-CDH-MSCV-cG reporter vector (System Biosciences, CA, USA) to obtain stable CopGFP-expressing pSLC (referred to as GFP$^+$ pSLC).

Gene and Protein Expression Analyses

Microarray, protein array, and qPCR analyses are detailed in the Extended Experimental Procedures and Table S3.

pSLC Differentiation to Mesenchymal Tissues

We employed established protocols for bone and adipocyte differentiation from mesenchymal stem cells (Pittenger et al., 1999). Myogenic differentiation with C2C12 myoblasts was performed as described (Shi et al., 2004). Detailed descriptions are available in the Extended Experimental Procedures.

In Vivo GFP$^+$ pSLC Transplantation to Skeletal Muscles and Dissemination of Infections

CD-1/nude mice (6–8 weeks, Charles-River) were preinjured with cardiotoxin-1 24 hr prior to the administration of ML-infected GFP$^+$ pSLC or GFP$^+$ Schwann cells. Each indicated experiment was performed with 5–6 mice per experimental group by repeating at least 3–4 times. Experimental details are in the Extended Experimental Procedures.

Macrophage-pSLC Cocultures, Migration Assays, and In Vitro Granuloma Formation

Detailed descriptions of experimental procedures of macrophage isolation and cocultures and in vitro granuloma formation are described in the Extended Experimental Procedures.

SUPPLEMENTAL INFORMATION

Supplemental Information includes Extended Experimental Procedures, seven figures, three tables, and one data file and can be found with this article online at http://dx.doi.org/10.1016/j.cell.2012.12.014.

ACKNOWLEDGMENTS

We thank Ian Wilmut and Emil Gotschlich for critical reading of the manuscript. We are grateful to Emil Gotschlich, Paul Nurse, Michael Young, Vincent Fischetti, Thomas Sakmar (Rockefeller University), John Savill, Jonathan Sackl, Nick Hastie (University of Edinburgh), and James Krahenbuhl (National Hansen's Disease Programs; NHDP) for their support during the initial and final phases of this study. Our thanks to Richard Truman (NHDP) for providing Fite's

(B–E) Macrophages were added to infected pSLC aggregates, incubated for 6 hr, 18 hr (B), 72 hr (C), and 96 hr (D), and labeled with antibodies to PGL-1 and macrophage markers F4/80 and CD11b. Shown are confocal images after 3D reconstructions (B); arrows (top panel) indicate phagocytosed ML-infected pSLC (green; ML in red) by macrophages (blue) within GLS. At 18 hr, a high number of ML (green) was found in macrophages (blue) that penetrated into GLS (B, bottom left panels). Occasional TUNEL$^+$ cells (red; 0.04%) were also found in these GLS (nuclei are shown in yellow). Bacterial transfer from GFP$^+$ pSLC to F4/80$^+$ macrophages (red) was also seen outside GLS (B, bottom right). (C) At 72 hr, more macrophages (blue) were incorporated into GLS, and ML were taken up by these macrophages (arrows); note less PGL$^+$ML in pSLC (left and middle panels) and departure of some macrophages carrying ML with them; yellow arrows depict macrophages carrying both pSLC debries and ML (right panels). (D) Disintegration of GLS and the release of ML-laden macrophages (arrows). (E) Correlation coefficients of bacterial transfer from pSLC to macrophages over time based on bacterial presence or absence (+/−ML) in pSCL (green) and in macrophages (blue).

(F) The proposed model: Schwann cells in the adult PNS infected with ML undergo a reprogramming process that converts Schwann cells to pSLC that promote bacterial dissemination. BNB: blood nerve barrier.

Scale bars, (A) 5 μm; (B–D) 20 μm.

staining of infected mouse tissue sections; members of the core facilities at the Rockefeller University and the University of Edinburgh for their invaluable assistance; Joe Dybaas, Jennifer Smith, Clara Eastby, Paola Basilico, and Maxmilien Grandclaudon (Rambukkana laboratory) for their participation and technical assistance; and members of Genome Exploration and EpigenDx for technical assistance and data analysis. *Mycobacterium leprae* were provided by The Laboratory Research Branch of NHDP, Baton Rouge, LA with funding from The American Leprosy Missions and the Hospitaler Order of St. Lazarus of Jerusalem. This work was funded in part by grants from NIAID (AI45816) and NINDS (NS45187), The Order of MALTALEP Foundation, The Rockefeller University, and the University of Edinburgh.

Received: July 9, 2012
Revised: October 31, 2012
Accepted: December 10, 2012
Published: January 17, 2013

REFERENCES

Bold, T.D., and Ernst, J.D. (2009). Who benefits from granulomas, mycobacteria or host? Cell *136*, 17–19.

Buatois, V., Fagète, S., Magistrelli, G., Chatel, L., Fischer, N., Kosco-Vilbois, M.H., and Ferlin, W.G. (2010). Pan-CC chemokine neutralization restricts splenocyte egress and reduces inflammation in a model of arthritis. J. Immunol. *185*, 2544–2554.

Chargé, S.B., and Rudnicki, M.A. (2004). Cellular and molecular regulation of muscle regeneration. Physiol. Rev. *84*, 209–238.

Chiu, B.C., Freeman, C.M., Stolberg, V.R., Hu, J.S., Komuniecki, E., and Chensue, S.W. (2004). The innate pulmonary granuloma: characterization and demonstration of dendritic cell recruitment and function. Am. J. Pathol. *164*, 1021–1030.

Cole, S.T., Eiglmeier, K., Parkhill, J., James, K.D., Thomson, N.R., Wheeler, P.R., Honoré, N., Garnier, T., Churcher, C., Harris, D., et al. (2001). Massive gene decay in the leprosy bacillus. Nature *409*, 1007–1011.

Davis, J.M., and Ramakrishnan, L. (2009). The role of the granuloma in expansion and dissemination of early tuberculous infection. Cell *136*, 37–49.

Eminli, S., Utikal, J., Arnold, K., Jaenisch, R., and Hochedlinger, K. (2008). Reprogramming of neural progenitor cells into induced pluripotent stem cells in the absence of exogenous Sox2 expression. Stem Cells *26*, 2467–2474.

Falkow, S. (1991). Bacterial entry into eukaryotic cells. Cell *65*, 1099–1102.

Fawcett, J.W., and Keynes, R.J. (1990). Peripheral nerve regeneration. Annu. Rev. Neurosci. *13*, 43–60.

Finzsch, M., Schreiner, S., Kichko, T., Reeh, P., Tamm, E.R., Bösl, M.R., Meijer, D., and Wegner, M. (2010). Sox10 is required for Schwann cell identity and progression beyond the immature Schwann cell stage. J. Cell Biol. *189*, 701–712.

Flynn, J.L., and Chan, J. (2001). Immunology of tuberculosis. Annu. Rev. Immunol. *19*, 93–129.

Gupta, J.C., Jesupadam, T., Gupta, M.C., and Gupta, D.K. (1975). A histopathologic study of striated muscle biopsies in leprosy. Int. J. Lepr. Other Mycobact. Dis. *43*, 348–355.

Gurdon, J.B. (1962). Adult frogs derived from the nuclei of single somatic cells. Dev. Biol. *4*, 256–273.

Gurdon, J.B., and Melton, D.A. (2008). Nuclear reprogramming in cells. Science *322*, 1811–1815.

Hoogduijn, M.J., Popp, F., Verbeek, R., Masoodi, M., Nicolaou, A., Baan, C., and Dahlke, M.H. (2010). The immunomodulatory properties of mesenchymal stem cells and their use for immunotherapy. Int. Immunopharmacol. *10*, 1496–1500.

Jessen, K.R., and Mirsky, R. (2005). The origin and development of glial cells in peripheral nerves. Nat. Rev. Neurosci. *6*, 671–682.

Job, C.K. (1989). Nerve damage in leprosy. Int. J. Lepr. Other Mycobact. Dis. *57*, 532–539.

Kaur, S., Malik, A.K., and Kumar, B. (1981). Pathologic changes in striated muscles in leprosy. Lepr. India *53*, 52–56.

Klopp, A.H., Gupta, A., Spaeth, E., Andreeff, M., and Marini, F., 3rd. (2011). Concise review: Dissecting a discrepancy in the literature: do mesenchymal stem cells support or suppress tumor growth? Stem Cells *29*, 11–19.

Lahiri, R., Randhawa, B., and Krahenbuhl, J.L. (2010). Infection of mouse macrophages with viable Mycobacterium leprae does not induce apoptosis. J. Infect. Dis. *201*, 1736–1742.

Le, N., Nagarajan, R., Wang, J.Y., Araki, T., Schmidt, R.E., and Milbrandt, J. (2005). Analysis of congenital hypomyelinating $Egr2^{Lo/Lo}$ nerves identifies Sox2 as an inhibitor of Schwann cell differentiation and myelination. Proc. Natl. Acad. Sci. USA *102*, 2596–2601.

Lee, J., Sayed, N., Hunter, A., Au, K.F., Wong, W.H., Mocarski, E.S., Pera, R.R., Yakubov, E., and Cooke, J.P. (2012). Activation of innate immunity is required for efficient nuclear reprogramming. Cell *151*, 547–558.

Li, Y., Chen, S., Yuan, J., Yang, Y., Li, J., Ma, J., Wu, X., Freund, M., Pollok, K., Hanenberg, H., et al. (2009). Mesenchymal stem/progenitor cells promote the reconstitution of exogenous hematopoietic stem cells in Fancg-/- mice in vivo. Blood *113*, 2342–2351.

Mani, S.A., Guo, W., Liao, M.J., Eaton, E.N., Ayyanan, A., Zhou, A.Y., Brooks, M., Reinhard, F., Zhang, C.C., Shipitsin, M., et al. (2008). The epithelial-mesenchymal transition generates cells with properties of stem cells. Cell *133*, 704–715.

Miko, T.L., Le Maitre, C., and Kinfu, Y. (1993). Damage and regeneration of peripheral nerves in advanced treated leprosy. Lancet *342*, 521–525.

Modlin, R.L., and Rea, T.H. (1988). Immunopathology of leprosy granulomas. Springer Semin. Immunopathol. *10*, 359–374.

Mosser, D.M., and Edwards, J.P. (2008). Exploring the full spectrum of macrophage activation. Nat. Rev. Immunol. *8*, 958–969.

Napoli, I., Noon, L.A., Ribeiro, S., Kerai, A.P., Parrinello, S., Rosenberg, L.H., Collins, M.J., Harrisingh, M.C., White, I.J., Woodhoo, A., and Lloyd, A.C. (2012). A central role for the ERK-signaling pathway in controlling Schwann cell plasticity and peripheral nerve regeneration in vivo. Neuron *73*, 729–742.

Ng, V., Zanazzi, G., Timpl, R., Talts, J.F., Salzer, J.L., Brennan, P.J., and Rambukkana, A. (2000). Role of the cell wall phenolic glycolipid-1 in the peripheral nerve predilection of Mycobacterium leprae. Cell *103*, 511–524.

Pearson, J.M., Rees, R.J., and Weddell, A.G. (1970). Mycobacterium leprae in the striated muscle of patients with leprosy. Lepr. Rev. *41*, 155–166.

Pittenger, M.F., Mackay, A.M., Beck, S.C., Jaiswal, R.K., Douglas, R., Mosca, J.D., Moorman, M.A., Simonetti, D.W., Craig, S., and Marshak, D.R. (1999). Multilineage potential of adult human mesenchymal stem cells. Science *284*, 143–147.

Polyak, K., and Weinberg, R.A. (2009). Transitions between epithelial and mesenchymal states: acquisition of malignant and stem cell traits. Nat. Rev. Cancer *9*, 265–273.

Qiu, B., Frait, K.A., Reich, F., Komuniecki, E., and Chensue, S.W. (2001). Chemokine expression dynamics in mycobacterial (type-1) and schistosomal (type-2) antigen-elicited pulmonary granuloma formation. Am. J. Pathol. *158*, 1503–1515.

Rambukkana, A. (2010). Usage of signaling in neurodegeneration and regeneration of peripheral nerves by leprosy bacteria. Prog. Neurobiol. *91*, 102–107.

Rambukkana, A., Salzer, J.L., Yurchenco, P.D., and Tuomanen, E.I. (1997). Neural targeting of Mycobacterium leprae mediated by the G domain of the laminin-alpha2 chain. Cell *88*, 811–821.

Rambukkana, A., Yamada, H., Zanazzi, G., Mathus, T., Salzer, J.L., Yurchenco, P.D., Campbell, K.P., and Fischetti, V.A. (1998). Role of alpha-dystroglycan as a Schwann cell receptor for Mycobacterium leprae. Science *282*, 2076–2079.

Rambukkana, A., Zanazzi, G., Tapinos, N., and Salzer, J.L. (2002). Contact-dependent demyelination by Mycobacterium leprae in the absence of immune cells. Science *296*, 927–931.

Scollard, D.M., Adams, L.B., Gillis, T.P., Krahenbuhl, J.L., Truman, R.W., and Williams, D.L. (2006). The continuing challenges of leprosy. Clin. Microbiol. Rev. *19*, 338–381.

Shetty, V.P., Antia, N.H., and Jacobs, J.M. (1988). The pathology of early leprous neuropathy. J. Neurol. Sci. *88*, 115–131.

Shi, D., Reinecke, H., Murry, C.E., and Torok-Storb, B. (2004). Myogenic fusion of human bone marrow stromal cells, but not hematopoietic cells. Blood *104*, 290–294.

Stoner, G.L. (1979). Importance of the neural predilection of Mycobacterium leprae in leprosy. Lancet *2*, 994–996.

Takahashi, K., and Yamanaka, S. (2006). Induction of pluripotent stem cells from mouse embryonic and adult fibroblast cultures by defined factors. Cell *126*, 663–676.

Tapinos, N., and Rambukkana, A. (2005). Insights into regulation of human Schwann cell proliferation by Erk1/2 via a MEK-independent and p56Lck-dependent pathway from leprosy bacilli. Proc. Natl. Acad. Sci. USA *102*, 9188–9193.

Tapinos, N., Ohnishi, M., and Rambukkana, A. (2006). ErbB2 receptor tyrosine kinase signaling mediates early demyelination induced by leprosy bacilli. Nat. Med. *12*, 961–966.

Theise, N.D., and Wilmut, I. (2003). Cell plasticity: flexible arrangement. Nature *425*, 21.

Tidball, J.G., and Villalta, S.A. (2010). Regulatory interactions between muscle and the immune system during muscle regeneration. Am. J. Physiol. Regul. Integr. Comp. Physiol. *298*, R1173–R1187.

Truman, R.W., and Krahenbuhl, J.L. (2001). Viable M. leprae as a research reagent. Int. J. Lepr. Other Mycobact. Dis. *69*, 1–12.

Weider, M., Küspert, M., Bischof, M., Vogl, M.R., Hornig, J., Loy, K., Kosian, T., Müller, J., Hillgärtner, S., Tamm, E.R., et al. (2012). Chromatin-remodeling factor Brg1 is required for Schwann cell differentiation and myelination. Dev. Cell *23*, 193–201.

Werneck, L.C., Teive, H.A., and Scola, R.H. (1999). Muscle involvement in leprosy. Study of the anterior tibial muscle in 40 patients. Arq. Neuropsiquiatr. *57*(3B), 723–734.

Wilmut, I., Schnieke, A.E., McWhir, J., Kind, A.J., and Campbell, K.H. (1997). Viable offspring derived from fetal and adult mammalian cells. Nature *385*, 810–813.